ChemComm

Accepted Manuscript

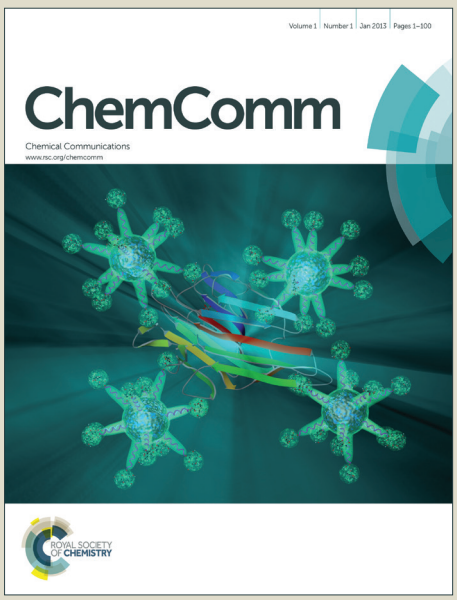

ROYAL SOCIETY OF CHEMISTRY

www.rsc.org/chemcomm

Cite this: DOI: 10.1039/c0xx00000x

www.rsc.org/xxxxxx

ARTICLE TYPE

Immobilizing Ni nanoparticles to mesoporous silica with size and location control via a polyol-assisted route for coking- and sintering-resistant dry reforming of methane

Ting Xie, Liyi Shi, Jianping Zhang and Dengsong Zhang*

Received (in XXX, XXX) XthXXXXXXXXX 20XX, Accepted Xth XXXXXXXXX 20XX
DOI: 10.1039/b000000x

The highly dispersed Ni nanoparticles in mesoporous silica were achieved *via* using polyol as new delivery conveyors and removable carbon templates. The catalyst exhibits excellent coking- and sintering-resistance in dry reforming of methane attributed to the controlled size and location of Ni nanoparticles.

The continuous rise of CO_2 concentration which mainly arises from the anthropogenic emission into the atmosphere has raised a worldwide concern. Dry reforming of methane reaction (DRM) appears to be attractive for the capacity to mitigate climate change through transforming the greenhouse gas into synthesis gas. Catalysts based on both noble and non-noble metal have been extensively applied in the DRM reaction. Wherein, Ni-based catalysts have been regarded as the most promising candidate because of their low cost and extensive supply.[1] Unfortunately, during the harsh reaction, the tendencies of Ni nanoparticles (NPs) sintering and carbon deposition are impediment for stable catalytic performance.[2] Therefore, from the standpoint of both academic and industrial, a kind of robust catalyst with excellent catalytic activity and durability is highly desired.

It is generally acknowledged that Ni NPs with small size can effectively suppress sintering and coking.[3, 4]Academic community has attempted numerous approaches to hinder the catalyst deactivation in the DRM reaction by controlling the size and distribution of Ni NPs.[5, 6] Because of the confinement effect of uniform channels and the high thermal stability, well-ordered mesoporous silica has been highlighted as an ideal support for the growth of metal NPs.[7, 8]Generally, this kind of supported catalyst is prepared by an incipient wetness route and the precursor aqueous solution infiltrates the hydrophilic channels of mesoporous silica by capillary force.[9] Nevertheless, the Ni precursor cannot be effectively delivered into the mesoporous channels. Therefore, the catalyst can't achieve simultaneous coke suppression and sintering-resistant while maintain excellent catalytic performance during high-temperature reactions.

Herein, we propose polyol such as ethylene glycol (EG) as new delivery conveyors and removable carbon templates to cast and *in situ* immobilize the nickel species into the channels of mesoporous silica. Specifically, the polyol coordinated with Ni^{2+} species could enter into the mesoporous channels easily by the capillary force, and then during the heat treatment under an inert atmosphere, the polyol decomposes to carbon. Carbon templates are the major contributors to highly dispersed Ni NPs, and simultaneously, they hinder Ni NPs' migrations from the internal surface of mesoporous channels to the outside and further inhibit the sintering.

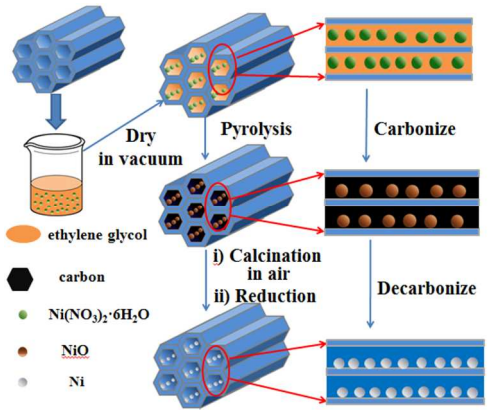

Fig.1 Schematic illustration of the catalyst Ni/SBA-15-EG

A schematic illustration of the synthetic pathway to mesoporous silicaSBA-15 confined Ni NPs catalyst is shown in Fig. 1. Firstly, the Ni precursor was delivered into the channels of SBA-15 by EG. In the following step, the intermediate product was dried in vacuum, and pyrolyzed in N_2. Finally, we obtained the catalyst SBA-15 supported highly dispersed Ni NPs *via* removing the carbon templates by being heated in air and *in-situ* reduction by a H_2-temperature programmed reduction (H_2-TPR) process. For comparison, we also prepare the catalyst identically via replacing EG by glycerol (GC), ethanol (EA) and H_2O.

The Transmission Electron Microscope (TEM) images show the morphologies of catalyst Ni/SBA-15-EG before (Fig. S1, ESI†) and after removing the carbon templates (Fig. 2A) and the Raman spectrum (Fig. S2, ESI†) proves the formation of carbon templates. Ni NPs are almost anchored into the well-ordered mesoporous channels, indicating that the introduction of EG restricts the location of Ni NPs. It is considerably beneficial to enhancing the sintering-resistance of the catalyst due to the confinement effect arising from the mesoporous wall of silica support.[10, 11]Better still, as the particle size distribution histogram (Fig. 2C) shown that these Ni NPs feature an ideal

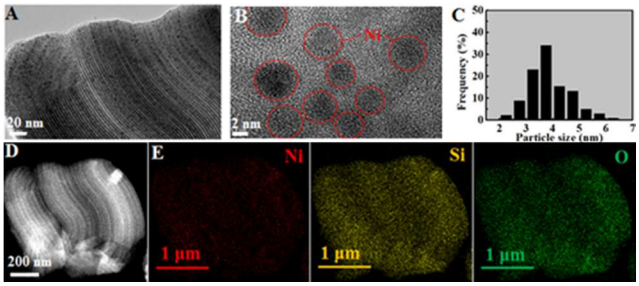

Fig.2 A. TEM image of Ni/SBA-15-EG; B. HRTEM image of Ni NPs in catalyst Ni/SBA-15-EG; C. Ni particle size distribution of Ni/SBA-15-EG; D. HAADF-STEM image of the Ni/SBA-15-EG catalyst; E. EDS mapping of Ni/SBA-15-EG catalyst

distribution for coke-resistant catalyst. That is, distributing uniformly with a narrow scope of size from 2.1-6.2 nm, and the Ni NPs approximate 3.6nm in average size are far smaller than those exhibiting a maximum centered at 8-9 nm for the catalyst Ni/SBA-15-H_2O which is prepared by an incipient wetness route (Fig. S4d, ESI†). The small size of Ni NPs is advantageous in the formation of more catalytic active sites, resulting in giving high activity in dry reforming of methane.[12] Meanwhile, the small Ni NPs arrange in the channels uniformly and isolate from each other, so it is deduced that the active sites of Ni NPs can be totally exposed to reactant gases. The morphology of catalyst Ni/SBA-15-EG is further investigated by high resolution transmission electron microscope (HRTEM) and high angle annular dark field-scanning electron microscope (HAADF-STEM) (Fig. 2B, D). They both exhibit highly ordered array of Ni NPs embedded into long-range ordered mesoporous channels of silica support. The Energy Dispersive X-ray (EDX) spectrometry (Fig. 2E and the spectrum see ESI†, Fig. S3) also demonstrates that Ni NPs load in the mesoporous silica with a homogeneous dispersion. We also characterized the catalysts Ni/SBA-15- GC and Ni/SBA-15-EA, respectively (see the details in ESI†, Fig. S4b, c). As a result, EA can't play a part in the dispersion and embedment of Ni NPs, it should impute the insufficient alcoholic hydroxyl group and carbon source. GC acts well in delivering and anchoring the nickel species into the mesoporous channels. The excellent morphologies of Ni/SBA-15-EG and Ni/SBA-15-GC should improve the activity and stability in the DRM reaction. However, it may be difficult to diffuse and dry because of the high viscosity and boiling point of GC, and it may impact on the delivering and immobilizing for Ni NPs, so we regard EG as the best dispersant to deliver the nickel precursor into mesoporous channels. As a universal polyol-assisted route, EG can also deliver and immobilize the Ni NPs into the mesoporous channels of KIT-6 (Fig. S5, ESI†).

The catalytic performance for DRM reaction was tested from 450 °C to 800 °C. It comes to light that the DRM reaction is endothermic, as shown in Fig. 3A, the conversions of CO_2 and CH_4 both increase for the samples with the reaction temperature increasing, which is similar to the thermodynamic equilibrium conversions calculated by the previous scientists.[13] In addition, owing to accompanying reverse water-gas shift reaction,[14] the conversion of CO_2 is higher than that of CH_4, and H_2/CO ratios decrease with time on stream (Fig. S8, ESI†).Apparently observed, the Ni/SBA-15-EG performs superior catalytic activity than Ni/SBA-15-H_2O.Simultaneously,

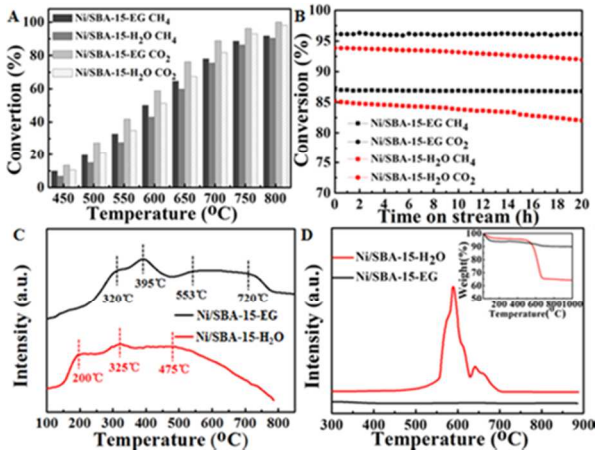

Fig. 3 A. CH_4 and CO_2 conversions at different temperatures for catalysts Ni/SBA-15-EG and Ni/SBA-15-H_2O; B. Catalysts conversions *versus* reaction time at 750 °C in the stability tests. C. H_2-TPR profiles of the fresh catalysts; D. O_2-TPO profiles of spent catalysts after stability test (inset: TG profiles of the spent catalysts)

the activity performances of the other two catalysts Ni/SBA-15-EAand Ni/SBA-15-GC are tested (Fig. S6, ESI†). The catalytic activities of Ni/SBA-15-EG and Ni/SBA-15-GC are higher than those of Ni/SBA-15-EA and Ni/SBA-15-H_2O, it could be attributed to the tiny and equably dispersed Ni NPs which afford more exposed active sites to the reactant gases.

The stability test of the catalysts with both high and low conversions were carried out at 750 °C (Fig. 3B and Fig. S7b, ESI†).The catalyst Ni/SBA-15-EG has a prolonged lifetime in the stability test with the steady TOF value of CH_4 (Table S1, ESI†), the catalytic activity does not change significantly after the harsh reaction. It could be explained in two aspects: the excellent sintering-resistance of Ni NPs and the enhanced coking-resistance of Ni NPs with small size. This can be verified by the TEM images, temperature programmed oxidation (TPO) and thermo gravimetric (TG) profiles of the spent sample as discussed in following sections. In contrast, in the case of Ni/SBA-15-H_2O, both the conversion of CH_4 and CO_2 decrease gradually with time on stream. The formation of larger Ni NPs leads to the sharp shrink of overall active surface areas and subsequently the catalytic activity decreases. During the long-term DRM reaction, carbon species deriving from the decomposition of CH_4 and Boudouard reaction generate. The larger facets and step edges of nickel particles facilitate the nucleation of amorphous carbon, it subsequently evolves into graphite carbon and then covers the active sites of Ni NPs.[15, 16] The diffusion of deposited coke generates carbon nanotubes which are responsible for the block of quartz tube after the long-term test. It further leads to sharp contact area decrease between the active metallic NPs and reactant gases, as a result, the deactivation of the catalyst occurs. Catalytic stabilities of the catalysts Ni/SBA-15-EA and Ni/SBA-15-GC under the identical reaction conditions are also evaluated (Fig.S7a, ESI†). The result is in accord with what we have deduced from the TEM characterization, Ni/SBA-15-GC and Ni/SBA-15-EG have enhanced coking- and sintering-resistance than Ni/SBA-15-EA and Ni/SBA-15-H_2O.

The H_2-TPR profiles are illustrated in Fig. 3C to depict the reduction behaviors of different catalysts. It has been demonstrated that $Ni^{2+}$is directly reduced to Ni^0 without any intermediate

oxidation state species,[17] hence, the different H_2 consumption peaks just take shape according to multitudinous NiO species. From TPR profiles, both samples mainly reflect the H_2 signal in three temperature regions, revealing the distinguished presence of three types of NiO species. Firstly, the peaks at low temperature zone from 200 ^oC to 350 ^oC are ascribed to bulk phase NiO grafted on the outside surfaces which have weak interaction with the support. Secondly, the moderate reduction peaks from 350 ^oC to 550 ^oC are associated with the NiO species which have relatively smaller particle diameter and enhanced interaction with the support. The size of NiO particles is also a crucial factor for reduction temperature probably owing to the surface energy.[18, 19] Thirdly, the tiny NiO particles embedded into the mesopore with intimate contact with the support are reducible at high temperature more than 600 ^oC. The TPR profile of Ni/SBA-15-EG displays that the reduction peaks mainly locate in moderate and high temperature regions, even appears at 720^oC, suggesting the metal-support interaction is strengthened with increased interfacial area between the tiny Ni NPs and support. It has made contribution to improving the catalytic performance in reforming process. While for the catalyst Ni/SBA-15-H_2O, the reflection peaks mainly settle at moderate and low temperature. The reason can be explained below, the aqueous solution of nickel precursor can hardly infiltrate into the mesoporous channels, leaving behind the NiO NPs grow bigger on the external surfaces of the support. Aggregation of NiO particles reduces the distribution and weakens the metal-support interaction. In addition, the reducibility of NiO species in Ni/SBA-15-GC is also stronger than that of those in Ni/SBA-15-EA and Ni/SBA-15-H_2O (Fig. S9, ESI†).

The TEM images and the corresponding histograms of the spent catalysts Ni/SBA-15-EG and Ni/SBA-15-GC after a long-term stability test (Fig.S10a, b, ESI†) verify our deduction that the sizes of metal NPs have not changed significantly after the rigorous reaction. The well-ordered mesoporous structure is covered by a thin graphene-like coke layer, while it is still maintained and the carbon nanotubes on the spent catalysts can hardly been observed. It has proved that the Ni NPs with small size possess a higher saturation concentration of carbonaceous species, so it can suppress carbon diffusion through the Ni NPs thanks to the lower driving force and then avoid the formation of carbon nanotubes.[20] Unluckily, the catalysts Ni/SBA-15-H_2O and Ni/SBA-15-EA haven't survived in the harsh reaction.

The amount of coke formation is evaluated by O_2-TPO and TG experiments (Fig. 3D). Apparently, there are two distinct CO_2 peaks in the spent catalyst Ni/SBA-15-H_2O, indicating the two types of coke: graphitic carbon and carbon nanotubes. The main form of coke is graphitic carbon which is responsible for the catalyst deactivation. Incredibly, detecting the spent Ni/SBA-15-EG in the same condition, the CO_2 signal can be neglected comparing with that of the spent Ni/SBA-15-H_2O. Similarly, the reflection peak of CO_2 associated with the amount of coke in catalyst Ni/SBA-15-GC also can't be detected (Fig. S11, ESI†). The less carbon deposition reveals the excellent coke-resistance for the catalysts Ni/SBA-15-EG and Ni/SBA-15-GC. The carbon deposited on the catalysts' surface after the long-term catalytic reaction was also quantified by TG measurements. Except the loss of adsorbed water, the weight loss of spent Ni/SBA-15-$H_2O$and Ni/SBA-15-EG are 32.3 % and 3.8 %, respectively, which agrees well with O_2-TPO.The higher coke deposition rate of Ni/SBA-15-H_2O (Fig.S12, ESI†) leads to its shorter lifetime.

To summarize, in this work, the catalyst Ni/SBA-15 was prepared by the polyol-assisted route and evaluated in the DRM reaction. The characterization result from TEM reveals that EG can successfully deliver and immobilize the nickel species into the channels of mesoporous silica. The high dispersion of Ni NPs for Ni/SBA-15-EG catalyst results in more active sites available for the reaction, and this leads to its higher catalytic activity. The confinement effect of pore walls plays a vital role in preventing the sintering of Ni NPs, and the Ni NPs with small size favor in enhancing the coking- and sintering-resistance so that Ni/SBA-15-EG presents higher and more stable catalytic performance. Our successful demonstration of supported tiny metal particles in mesoporous materials paves the way towards the other relevant nanocatalysts with enhanced durability which can be applied in many other catalytic reactions involving the coking- and sintering- resistance.

Notes and references

Research Center of Nano Science and Technology, Shanghai University, Shanghai 200444, China. E-mail: dszhang@shu.edu.cn; Fax: +86 21 66136079; Tel: +86 2166136081.

† Electronic Supplementary Information (ESI) available:Experimental details, TEM images, catalytic performance, H_2-TPR and TPO measurements.See DOI: 10.1039/b000000x/

1. L. V. Mattos, G. Jacobs, B. H. Davis and F. B. Noronha, *Chem Rev*, 2012, **112**, 4094-4123.
2. J. Lu, B. Fu, M. C. Kung, G. Xiao, J. W. Elam, H. H. Kung and P. C. Stair, *Science*, 2012, **335**, 1205-1208.
3. C. Zhang, W. Zhu, S. Li, G. Wu, X. Ma, X. Wang and J. Gong, *Chem Commun*, 2013, **49**, 9383-9385.
4. S. Li, C. Zhang, Z. Huang, G. Wu and J. Gong, *Chem Commun*, 2013, **49**, 4226-4228.
5. D. Baudouin, K. C. Szeto, P. Laurent, A. De Mallmann, B. Fenet, L. Veyre, U. Rodemerck, C. Coperet and C. Thieuleux, *J Am Chem Soc*, 2012, **134**, 20624-20627.
6. N. Wang, K. Shen, L. Huang, X. Yu, W. Qian and W. Chu, *ACS Catal.*, 2013, **3**, 1638-1651.
7. G. Prieto, J. Zečević,H. Friedrich, K. P. de Jong and P. E. de Jongh, *Nat. Mater.*, 2012, **12**, 34-39.
8. F. X. Zhu, W. Wang and H. X. Li, *J Am Chem Soc*, 2011, **133**, 11632-11640.
9. J. H. Park, S. K. Kim, H. S. Kim, Y. J. Cho, J. Park, K. E. Lee, C. W. Yoon, S. W. Nam and S. O. Kang, *Chem Commun*, 2013, **49**, 10832-10834.
10. J. Shi, *Chem Rev*, 2013, **113**, 2139-2181.
11. I. J. Morales, J. S. González,P. M. Torres, A. J. López, , *Appl. Catal., B*, 2011, **105**, 199-205.
12. S. He, C. Li, H. Chen, D. Su, B. Zhang, X. Cao, B. Wang, M. Wei, D. G. Evans and X. Duan, *Chem Mater*, 2013, **25**, 1040-1046.
13. M. C. J. Bradford, M. A. Vannice, *Catal. Rev*, 1999, **41**, 1-42.
14. C. Liu, J. Ye, J. Jiang and Y. Pan, *Chemcatchem*, 2011, **3**, 529-541.
15. Z. Liu, J. Zhou, K. Cao, W. Yang, H. Gao, Y. Wang and H. Li, *Appl. Catal., B*, 2012, **125**, 324-330.
16. X. Du, D. Zhang, R. Gao, L. Huang, L. Shi and J. Zhang, *Chem Commun*, 2013, **49**, 6770.
17. N. Wang, K. Shen, X. Yu, W. Qian and W. Chu, *Catal. Sci. Technol.*, 2013, **3**, 2278.
18. J. Hong, W. Chu,P. A. Chernavskii, A. Y. Khodakov, *J Catal*, 2010, **273**, 9–17.
19. C.T. Campbell, S. C. Parker,D. E. Starr, *Science*, 2002, **298**, 811-814.
20. S. Zhang, S. Muratsugu, N. Ishiguro and M. Tada, *ACS Catal.*, 2013, **3**, 1855-1864.